Optimal Frequency Bands for Modeling the Coupling of Structure-borne to Underwater Sound of a Surface Vessel

Andreas Galka, Jan Abshagen, Arne Stoltenberg and Volkmar Nejedl

Abstract

We present a method for investigating the coupling of structure-borne sound (SBS) and underwater sound (UWS) of ships based on a decomposition in optimal frequency bands. The coupling is modeled by a linear regression model for sequences of spectral power, integrated over frequency intervals and moving time windows. As part of this analysis, a novel approach to detecting frequency intervals that bear particular relevance for the relationship between SBS and UWS is introduced. Regression models are regularized by a maximum-significance constraint. Cross-correlations between UWS regressands and SBS regressors seem to be promising as quantitative measures for describing the coupling between SBS and UWS time series. The method is evaluated with experimental data recorded simultaneously from fixed SBS sensors on-board the research vessel PLANET and from a freely drifting buoy system during an open-sea experiment north of the Outer Hebrides, Scotland, in 2011.

Index Terms

Underwater sound, structure-borne sound, regularization, optimization.

I. Introduction

Sound that is radiated from a ship into the surrounding water is generated by a variety of sources located either in- or outside the ship's hull [1]. Flow or propeller noise are external hydrodynamical sources, while internal sources originating from machinery (engines, generators, or pumps) couple into the mechanical structure of a ship as structure-borne sound (SBS). SBS is transmitted through various pathways to the ship's hull and can ultimately radiate as underwater sound (UWS) into the far-field [2], [3]. Since underwater noise radiated from ships contributes substantially to the ambient noise in the ocean [4], [5], several measurements of the spectral level of cargo ships have been performed [6], [7], [8]. Despite the complexity of noise generation, the behavior of a ship as a sound source can beneficially be characterized by the *source level*, i.e., the spectral sound pressure level of a point source

A. Galka is with the Information and Coding Theory Lab, Technical Faculty, University of Kiel, 24098 Kiel, Germany.

J. Abshagen, A. Stoltenberg and V. Nejedl are with the Research Department for Underwater Acoustics and Marine Geophysics, Bundeswehr Technical Center WTD71-FWG, Berliner Straße 115, 24340 Eckernförde, Germany.

Manuscript received January 30th, 2016; accepted November 21th, 2016

at a (reference) distance of one meter [9], [10], [11]. According to this definition propagation effects, such as *Lloyd's Mirror Effect*, and losses due to, e.g., geometrical spreading or damping, are treated separately.

In principle, the radiation of sound from a (partly) submerged body, such as the underwater hull of a ship, can be calculated from the Kirchhoff-Helmholtz integral, given the normal velocity component of the hull vibrations and the surface pressure [3]. Due to this deep connection between surface sources and radiated sound field discrete representations of the Kirchhoff-Helmholtz integral have preferably been used in numerical modeling [12]. While information on hull vibrations of real ships are - at least partly - accessible from on-board measurements, more sophisticated techniques, such as acoustic holography [13], and a substantial experimental effort would be required for performing surface pressure measurements. Even though the (instantaneous) prediction of the underwater far-field signature of a ship is of large relevance in naval application, such approach seems unfeasible in operational situations. Therefore, for such applications prediction methods need to cope with the situation of incomplete information based only on on-board measurements of vibrations at a set of sensor positions, including main aggregates and certain positions on the hull. It is therefore desirable to investigate the coupling of structure-borne sound to the underwater sound of a ship and to utilize the information which is available on-board in an optimal way.

An experimental approach is given by performing experiments consisting of simultaneous recordings of both SBS and UWS. This paper is based on data recorded in August 2011 on the German research vessel (RV) PLANET under deep-water conditions, north of the Outer Hebrides [14]. Data resulting from such experiment consist of one set of multivariate SBS time series, recorded at a number of locations within the ship (in particular, at a subset of the hull frames), while the ship moves, and of another set of multivariate UWS time series, recorded from a linear array of hydrophones, suspended vertically from a floating buoy. The experiments were part of a collaboration of several NATO nations lead by CSSM [1] and DRDC [2] Atlantic [15]. Recording UWS data with horizontal arrays of hydrophones would also be desirable; however, performing such experiments under deep-water conditions would entail considerable additional effort, compared to vertical arrays, therefore it is rarely accomplished.

In this paper a methodology for data-driven modeling of the coupling of SBS and UWS time series is introduced, based on the approach of transforming measured data into a sequence of values of spectral power, integrated over a set of intervals in frequency domain, and a set of moving time windows. This approach represents an alternative to the possibly more straightforward, but also more challenging, approach of directly modeling the coupling of the sound data in the time domain. The coupling is modeled by a linear regression model for predicting the sequence of UWS spectral power values, as dependent variables, by the SBS spectral power values, as independent variables. As a distinctive feature of the proposed algorithm, the borders between the frequency intervals are not predefined, but obtained from the given data by a numerical optimization procedure. The function to be optimized is given by a regularized blend of the usual least-squares function and the corresponding expression for the significance of the regression parameters.

The structure of this paper is as follows: In section 2 the experimental setup is described, while the available

[1]German-Dutch *Centre for Ships Signature Management* located at WTD71

[2]Defense Research and Development Canada

SBS and UWS data are briefly presented in section 3. In section 4 the procedure for preprocessing is discussed. In section 5 the main regression model for sequences of spectral power is introduced. The optimization approach to estimating optimal frequency intervals is presented in section 6, while section 7 discusses practical aspects of the optimization. Section 8 presents the results; further discussion is provided in section 9. Finally, conclusions are given in the last section.

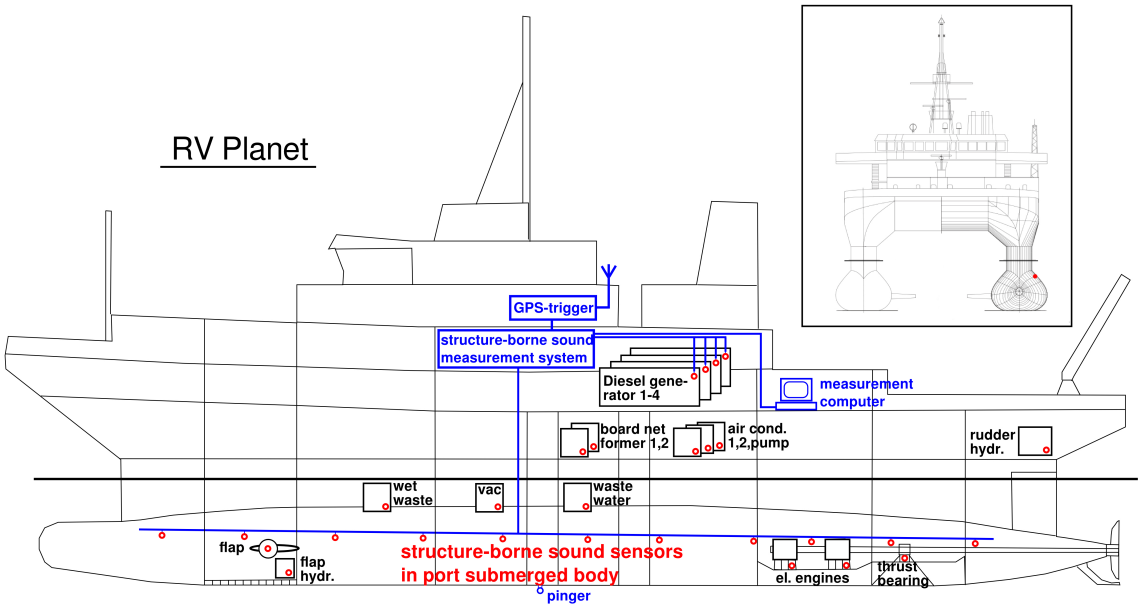

Fig. 1. Schematic drawing of RV PLANET in side view (port side) with main on-board instrumentation and measurement equipment. The SWATH design of PLANET can be seen in front view (inset).

II. Experimental setup

The experiments have been performed with RV PLANET in the Atlantic Ocean north of the Outer Hebrides (Scotland) in August 2011 [14]. At the measurement position outside the continental shelf region a water depth of more than 1000 m ensured acoustic free-field conditions to sufficient degree, such that effects from the bottom could be neglected. RV PLANET is a *Small Waterplane Area Twin Hull* (SWATH) ship designed especially for acoustics measurements at open sea. It has a length of 73.0 m, a width of 27.2 m, and a draft of 6.8 m. The displacement is 3500 tons. With a diesel-electric propulsion system a maximum speed of 15 knots can be achieved. In order to make the vessel quieter, the diesel engines are encapsulated and located on the main deck above the water surface. A schematic drawing of RV PLANET with the main machinery and the SBS measurement system is shown in Fig. 1.

RV PLANET is equipped with two types of SBS IEPE-sensors in the submerged body at its port side: Brüel & Kjær (BuK) 8325-A (a) and 5958 (b). The sensors are located pairwise at every 4th frame of the ship's hull structure, forming an approximately equally spaced line-array along the port hull (however, the sensors at frames 30, 34 and 38 were non-operational during the experiments). Distance between neighboring sensors is approximately 4 m on

average. The two types of sensors have sensitivities of 10.2 mV/ms^{-2} (a) resp. 1.0 mV/ms^{-2} (b), a frequency range from 1 Hz to 10 kHz (a) resp. 1 Hz to 11 kHz (b) and noise levels of 3 mm/s^2 (a) resp. $<$ 15 mm/s^2 (b) within their frequency range. The signal recording of the sensors was carried out with a modular Heim/Zodiac DataRec4 System capable of continously recording 128 sensors with 24 bit resolution at a nominal sampling rate of $f_{\mathrm{SBS}} = 50\,\mathrm{kHz}$.

In order to attach the SBS sensors to the frames, small cubic blocks of steel have been welded to the frames at positions forming a horizontal plane through the port submerged part of the ship (blue horizontal line and red dots in Fig. 1), in a way such that the faces of the blocks point towards horizontal and vertical directions; while the vertical direction is the same for all frames, the horizontal directions are different, depending on the local shape of the hull. At each block, two SBS sensors are glued to these faces, one in vertical direction and one in the local horizontal direction. Due to the curved shape of the hull (see insets in Figs. 1 and 2) the directions of these two sensors are not perpendicular to the hull, instead the horizontal directions form angles with the hull in the range of 30-70°, depending on position (i.e., frame number). However, since at each frame two perpendicular projections are recorded simultaneously, the local SBS component perpendicular to the hull can always be reconstructed.

Underwater sound was measured with a vertical hydrophone line array mounted to a freely drifting, autonomous buoy system, consisting of a radio buoy and a subsurface unit connected by an electro-optical cable. The array consists of an elastic hose containing 128 piezo-electric hydrophones (sensitivity: -201 dB (V/μPa)); resonance frequencies of hydrophones are far above the frequencies of interest for this paper. The hydrophones can be combined to three lines of 64 staves (nested array). These three lines are designed for different frequency ranges up to 5 kHz. The raw data are stored completely in the subsurface unit. Selected data can be transferred via WLAN to the laboratory at RV PLANET for quick visual analysis. The buoy system is controlled via WLAN, VHF-radio or ORBCOMM. The power supply allows an autonomous operating time up to 8 hours. The acoustic center of the hydrophone array was set to a water depth of about 43 m; through appropriate design of the buoyancy elements the depth position of the array is largely decoupled from surface waves. UWS data is recorded with 16 bit resolution at a nominal sampling rate of $f_{\mathrm{WS}} = 15625\,\mathrm{Hz}$. In order to achieve sufficient resolution for the frequency interval of interest, a prewhitening filter is applied, prior to A/D conversion. This filter has its 3dB point at 1 kHz and attenuates lower frequencies according to a f^2 characteristics; at 100 Hz the attenuation reaches 20 dB. More details on the design of the buoy system can be found in [14].

During the experiments, the vertical hydrophone line array was floating freely; due to an attached weight (50 kg), the array will approximately be oriented vertically. By coherence analysis of the raw UWS data, strong deviations from vertical orientation can be ruled out. However, for the method introduced in this paper, such deviations would not pose a problem, due to chosen beamformer design (see below).

III. Time series of structure-borne sound and underwater sound

For a single measurement "run" RV PLANET passed the buoy system on a straight track at constant speed. The UWS measurements were started and stopped about 1500 m before and after the closest point of approach (CPA); the SBS measurements took place during a shorter time interval, defined by a distance of approximately

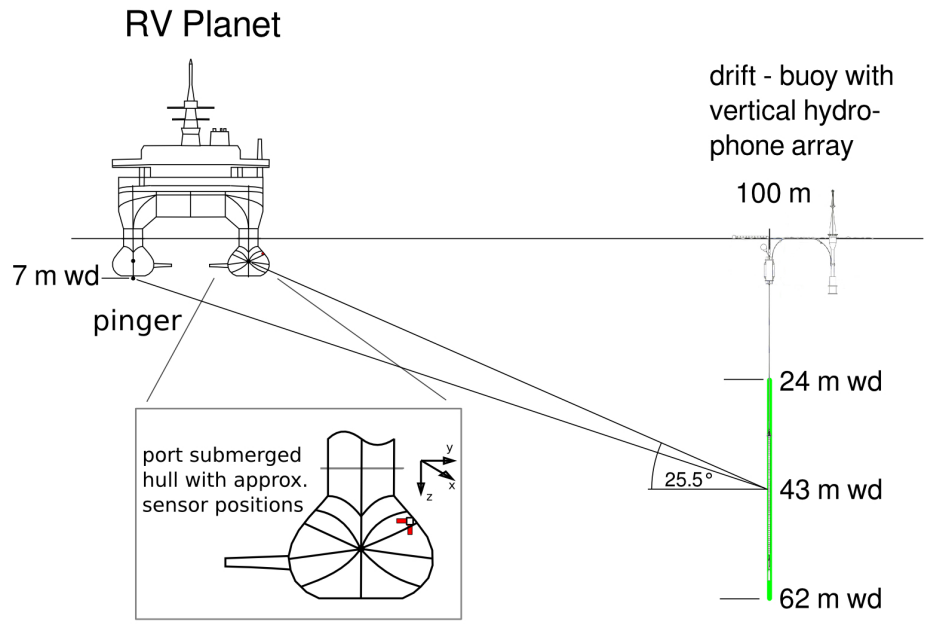

Fig. 2. Measurement setup at CPA in front view (wd: water depth): RV PLANET has a distance of about 100 m from the buoy system and the acoustics depth of the submerged hydrophone array is 43 m. PLANET is therefore *seen* from the array at an angle of about 25°, which allows suppression of ambient noise from the surface or from distant sources with focused beamforming. The hydrophone array consists of 128 hydrophones which are distributed over a length of 38 m (marked by green line) and can be combined to three lines of 64 staves (nested array). The inset at the left side shows the positions and orientations of the pairs of SBS sensors (red).

500 m before and after the CPA. For the example of a run with a speed of 6 knots this would correspond to time intervals of approximately 950 s (UWS) and 350 s (SBS). The distance between ship and buoy at CPA was approximately 100 m. The distance was estimated by (GPS triggered) LFM-pulses (chirps) emitted by an acoustical transducer (pinger) mounted to the bottom of the starboard hull. The center frequency of the pulses was 4 kHz with a bandwidth of 250 Hz; the length of a pulse was 0.1 s, and the repetition rate was 0.1 Hz. The frequency range of the pinger is well above the frequency range of interest for this paper. In naval applications, the range of frequencies up to 500 Hz is most relevant for prediction, since within this range sound is propagated well into large distance. The measurement setup at CPA is displayed in Fig. 2.

The available data from each single run consists of 24 paired data sets of SBS time series and UWS time series, each spanning the sequence of the ship approaching the submerged array, passing it and leaving it behind. In this paper, only the SBS data sets measured on the hull frames are taken into account, since underwater sound is radiated from the hull into the surrounding water. A set of five runs has been selected, and within each run only an interval of 8 s length around the CPA is analyzed; however, the presented methodology can be applied easily to arbitrarily chosen intervals. Using only data recorded around the CPA offers the advantage of better signal-to-noise ratio (SNR); furthermore, Doppler effects can be approximately neglected.

Table 1 provides a list of the selected runs. It contains the label of the run, the speed of the ship, the direction of

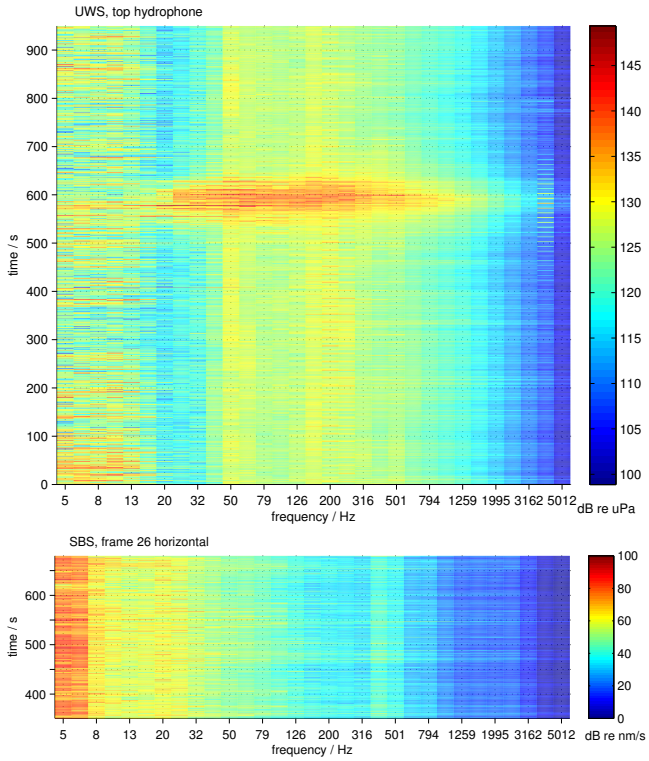

Fig. 3. Third octave spectrograms of the complete run 3P2A4: top hydrophone, water depth ≈ 24 m (top subfigure), and horizontal SBS sensor at frame 26 (bottom subfigure). The closest point of approach (CPA) occurs at time 570 s. In the top subfigure, power at low frequencies has been attenuated by a prewhitening filter (see text for details). Note that in the top subfigure in the highest frequency bins (right side of the figure) the periodical pinger signals are visible (repetition rate 0.1 Hz). SBS data was recorded only for a shorter time interval than UWS data; the vertical axis shows corresponding times in seconds.

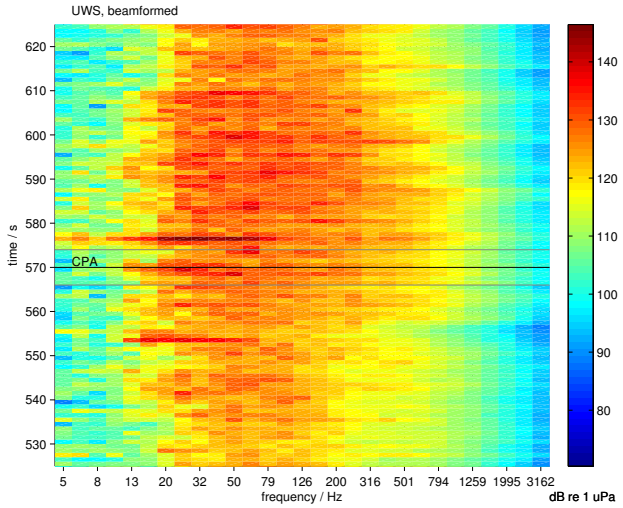

Fig. 4. Third octave spectrogram of the 100 s window of run 3P2A4 containing the closest point of approach (CPA): beamformed signal from all 128 hydrophones (focused beamformer). Again, power at low frequencies has been attenuated by a prewhitening filter. The CPA is denoted by the horizontal black line at time 570 s; the 8 s window around the CPA analyzed in this paper is denoted by a pair of grey lines.

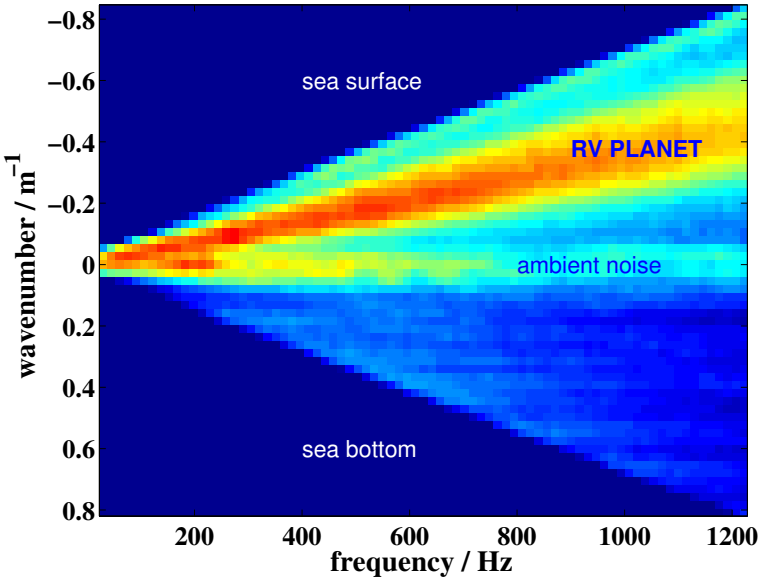

Fig. 5. Wavenumber-frequency spectrum at CPA of run 3P2A4, calculated on an 8 s window with a frequency resolution of 15.3 Hz, from a sub-array of 64 equally spaced hydrophones (spacing 0.6 m). Hamming windowing was applied in both temporal and spatial direction. The signal from RV PLANET can be clearly distinguished from that of other sources (ambient noise, sea surface), from its different angle of incidence. Due to a water depth in excess of 1000 m, no signals from the sea bottom are visible.

movement (with or against swell), the position of the buoy relative to the ship (in most cases port side) and further information on the physical state of the ship.

The UWS third octave spectrogram for a complete run is displayed in Figs. 3 and 4; while Fig. 3 (top subfigure) shows a spectrogram for the recordings at the top single hydrophone, Fig. 4 shows the spectrogram for a close-up of the 100 s window around the CPA, using a beamformed signal from all 128 hydrophones. In the figures various typical features of UWS recordings can be seen, such as the increased levels at the CPA (which occurs at time 570 s), but also the periodical pinger signals at 4 kHz. In Fig. 4, at higher frequency some traces of a spatial mode structure can be seen. Note that emission of UWS is asymmetrical with respect to time: in the figures, the major part of the UWS power is visible after the CPA, i.e., on the length scales probed by a measurement run, the majority of UWS power is emitted in backward direction. For comparison, also for one SBS hull sensor (frame 26, horizontal), a third octave spectrogram is shown (Fig. 3, bottom subfigure); note that SBS power spectra do not display major changes, since the state of the ship was kept constant during each run.

In addition, in Fig. 5 we show for the same run a wavenumber-frequency spectrum for the frequency range $[0\ 1200]$ Hz, at the CPA. A wavenumber-frequency analysis allows the separation of UWS sources with different angles of incidence. In the figure, it can be seen that while the dominant signal corresponds to RV PLANET, other signals are also present. Disturbing noise originates, for instance, from the sea surface, but also from distant sources (in the figure denoted as “ambient noise”). Due to sound channel propagation, distant sources can severely disturb a measurement. However, the resulting directivity of ambient noise allows a separation of the ship from distant sources. In practice, since at the CPA the distance between array and ship is rather small, this separation

can preferably be performed by a focused beamformer.

run	speed / knots	rotations / min.	active diesel generators	swell	aspect buoy
3P2A4	6	55	3	against	starboard side
3P6B1	8	75	2	with	port side
3P6B3	8	65	2	with	port side
3P3B3	15	140	1,2,3,4	with	port side
3P3B5	15	140	1,2,3,4	with	port side

TABLE I

LABELS AND ESSENTIAL CONDITIONS OF THE RUNS SELECTED FOR THIS PAPER.

IV. PREPROCESSING

Prior to any specific attempt at modeling the relationship between SBS and UWS, several preprocessing steps need to be applied:

1) Since both data sets within each run have been recorded with different sampling rates, they have to be mapped to a common sampling rate; in this case the lower sampling rate of UWS, 15625 Hz, was chosen.
2) Both data sets need to be aligned with respect to time. This is possible up to a precision of one second by using the GPS signals recorded within both data sets. A further improvement is obtained by explicitly aligning the signals of the pinger which is mounted to the bottom of the starboard hull. This alignment will also provide a small correction of the sampling rate of SBS, assuming that the sampling rate of UWS is correct. The correction is recomputed for each run. Furthermore, the delay due to signal propagation from the ship to the array can be removed during this step.
3) The dimensionalities of both data sets need to be reduced. For UWS, this can be achieved conveniently by employing a (focused) beamformer, such that the 128 raw data channels are merged into a one-dimensional representation. Within each window of 8 s length, the beamformer steers on the direction towards the pinger, and thereby the ship. As additional benefits of beamforming we mention an improved signal-to-noise ratio and the suppression of water sound components arriving from other directions, as discussed above.

   For SBS, an extensive correlation analysis has been carried out, employing linear models such as *Principal Component Analysis* (PCA) and *Independent Component Analysis* (ICA), and clustering approaches based on the power spectrum, in an attempt to find a representation with reduced dimensionality. However, it was found that altogether the amount of redundancy within the set of SBS sensors was quite limited, such that no significant reduction of dimensionality could be achieved. It was then decided to include only the $N = 24$ operational SBS sensors on the hull frames of the port side hull into the further analysis. We assume that these are the most relevant positions for the purpose of investigating the coupling of SBS to UWS.

V. ANALYSIS OF FLUCTUATIONS OF SPECTRAL POWER

We are now in a position to describe the main methodology for investigating the coupling of SBS time series to UWS time series. Since a straightforward analysis of cross-correlation was found to be unsuitable, we proceed as

follows.

Let $x(t,c)$ denote the SBS data at time $t\,, t = 1, \ldots, T$, and SBS sensor channel $c\,, c = 1, \ldots, N$, and let $y(t)$ denote the beamformed UWS data at time t. Using the pinger signal, time has been shifted such that propagation delays are approximately removed. However, we emphasize that due to the physical extension of the ship, there will still be various unknown delays between different sound sources and the SBS sensors.

Within the chosen time interval (which is always chosen around the CPA) we divide the data further into a set of W short windows of equal length. Furthermore we divide the frequency axis into V intervals

$$[f_1\ f_2], [f_2\ f_3], \ldots, [f_V\ f_{V+1}] \tag{1}$$

where $f_1 = 0\,\text{Hz}$ and $f_{V+1} = 500\,\text{Hz}$. Since the range of frequencies up to 500 Hz is most relevant for prediction in naval applications, higher frequencies are not studied in the analysis discussed in this paper. For later use, we shall collect the variable parameters of the corresponding partition of the interval $[f_1\ f_{V+1}]$ in a vector $\mathbf{v} = (f_2, \ldots, f_V)$; note that f_1 and f_{V+1} are fixed, therefore they are excluded from $\mathbf{v}$.

For each window $w\,, w = 1, \ldots, W$, each frequency interval $[f_v\ \ f_{v+1}]\,, v = 1, \ldots, V$, and each chosen SBS sensor channel $c\,, c = 1, \ldots, N$, the spectral power is computed by summing up the absolute-square of the Discrete Fourier Transform $\mathcal{F}$ of the SBS data within the wth window:

$$P^{\text{SBS}}(w, v, c) = \sum_{[f_v\ f_{v+1}]} \mathcal{F}\big(x(t,c)\big)^* \mathcal{F}\big(x(t,c)\big) \tag{2}$$

The length of the windows, the sampling frequency and the maximum frequency f_{V+1} determine the spectral resolution that can be achieved within the interval $[f_1\ \ f_{V+1}]$. For the given sampling rate of 15625 Hz and a window length of 4096 samples, a spectral resolution of $F = 131$ Fourier bins within the interval $[0\ \ 500]\,\text{Hz}$ is obtained. From each data window to be analyzed, the mean is removed first, such that no power at zero frequency is retained. For a total interval length of 8 s, the number of windows results as $W = 30$.

As a result, a sequence of values of integrated spectral power $P^{\text{SBS}}(w, v, c)$ is obtained, for each frequency interval $[f_v\ \ f_{v+1}]\,, v = 1, \ldots, V$, and each SBS sensor $c\,, c = 1, \ldots, N$. The same procedure is also applied to the beamformed UWS time series, resulting in a corresponding sequence of values of integrated spectral power $P^{\text{UWS}}(w, v)$.

We now aim at detecting correlations between SBS and UWS by studying the fluctuations of $P^{\text{UWS}}(w, v)$ as a function of the $P^{\text{SBS}}(w, v, c)$. Within the chosen time interval of 8 s length, the power within each frequency interval will display fluctuations, resulting from changes of the internal state of the ship or randomly occuring interactions of the ship with the water, and these fluctuations will be reflected both in the SBS and the UWS time series. Since the ship is the origin of the UWS that is recorded by the hydrophone array (after beamforming), we model $P^{\text{UWS}}(w, v)$, as a dependent variable, by the set of $P^{\text{SBS}}(w, v, c)$, as independent variables.

For the actual modeling, we need to normalize the dependent and independent variables to zero mean and unit variance; from now on, $P^{\text{UWS}}(w, v)$ and $P^{\text{SBS}}(w, v, c)$ shall refer to sequences of integrated spectral power that have already been normalized. The model is then set up as a linear instantaneous least-squares (LS) model

$$P^{\text{UWS}}(w, v) = \sum_{c=1}^{N} \beta(c, v) P^{\text{SBS}}(w, v, c) + \epsilon(w, v) \tag{3}$$

where $\beta(c, v)$ denotes a set of regression coefficients, to be estimated by standard techniques for LS modeling. Alternatively, they can be estimated by robust techniques [16]; for the results reported in this paper, we have always applied both the standard and the robust algorithm, but did not find significant differences in any case.

In equation (3), $\epsilon(w, v)$ denotes a sequence of regression residuals. We can define an overall LS model residual variance from $\epsilon(w, v)$ by

$$\sigma^2_{\mathrm{LS}}(\mathbf{v}) = \frac{1}{VW - 1} \sum_{w=1}^{W} \sum_{v=1}^{V} \epsilon^2(w, v) \quad . \tag{4}$$

Furthermore, the step of estimating the regression coefficients also provides us with estimates of the corresponding standard deviations $\sigma_\beta(c, v)$. By dividing the absolute values of the estimates of the regression coefficients $\hat{\beta}(c, v)$ by the estimates of the standard deviations $\hat{\sigma}_\beta(c, v)$, the t-value can be computed:

$$t(c, v) = \frac{|\hat{\beta}(c, v)|}{\hat{\sigma}_\beta(c, v)} \tag{5}$$

We find it convenient to define a mean squared t-value by

$$\overline{t^2}_{\mathrm{LS}}(\mathbf{v}) = \frac{1}{VN} \sum_{c=1}^{N} \sum_{v=1}^{V} t^2(c, v) \tag{6}$$

This value can be employed for the purpose of quantifying the average significance of the set of regression coefficients of a given LS model.

We emphasize that the regression approach presented in this paper tacitly assumes that the relationship between SBS and UWS remains constant during the 8 s time interval around the CPA. In future work it should be investigated whether this assumption is justified.

VI. Estimation of optimal frequency intervals

While describing the LS modeling approach in the preceding section, we have assumed that a set of frequency intervals $(f_v \; f_{v+1}), v = 1, \ldots, V$, was given. However, it is not obvious how this set should be chosen. One may select certain intervals according to prior information on relevant frequency lines or frequency bands in SBS and UWS time series. In a purely data-driven approach it would be preferable to let the data themselves decide on optimal frequency intervals. This idea can be implemented by an optimization approach.

We choose the following function to be maximized:

$$\phi_\lambda(\mathbf{v}) = \lambda \log\big(\overline{t^2}_{\mathrm{LS}}(\mathbf{v})\big) - \log\big(\sigma^2_{\mathrm{LS}}(\mathbf{v})\big) \tag{7}$$

This function consists of two terms, the second of which corresponds to standard LS modeling, while the first term represents an additional constraint on the optimization, namely the constraint that the average significance of the set of regression coefficients also be maximized. Equation (7) represents a regularization approach to combining these two optimization tasks, where the *regularization parameter* λ controls the relative influence of the two tasks.

The case of small values of λ corresponds to the minimization of $\sigma^2_{\mathrm{LS}}(\mathbf{v})$ i.e., the standard LS case, such that the accuracy of modeling the data is maximized; however, this function does not pay attention to the significance of the regression coefficients. On the other hand, the case of large values for λ corresponds to maximizing the average significance of the set of regression coefficients of the model, i.e., maximizing $\phi_\lambda(\mathbf{v})$ results in models with

regression coefficients that differ from zero with highest possible significance. Medium values for λ correspond to a compromise between the maximization of $\overline{t^2}_{\mathrm{LS}}(\mathbf{v})$ and the minimization of $\sigma^2_{\mathrm{LS}}(\mathbf{v})$.

The value for the regularization parameter λ that is actually employed, may be chosen by techniques like finding the inflection point of the so-called *L-curve*, i.e., a plot of a set of pairs $\Big(\log\big(\overline{t^2}_{\mathrm{LS}}(\mathbf{v})\big), \log\big(\sigma^2_{\mathrm{LS}}(\mathbf{v})\big)\Big)$ which results from choosing a set of different values for λ.

We remark that the function $\phi_\lambda(\mathbf{v})$ does not contain any precaution against overfitting, i.e., using a model with excessively large number of model parameters. Increasing the number of frequency intervals V will gradually reduce $\sigma^2_{\mathrm{LS}}(\mathbf{v})$, without reaching an optimal value of V. In this paper we will not apply modifications against overfitting since we will employ preselected values for V.

VII. Optimization: practical aspects

In practical work, the number of frequency intervals V needs to be selected first. Then, $\mathbf{v} = (f_2, \ldots, f_V)$ will be a vector of model parameters with dimension $V - 1$. Optimal values for the parameters $f_2, \ldots, f_V$ cannot be estimated by conventional schemes for numerical optimization, such as the Levenberg-Marquardt or Gauss-Newton methods, since the frequency space is "quantized" into 131 bins that result from the limited length of the windows; as a result no meaningful gradients can be computed. Instead we employ a grid search approach [17].

For $V = 2$, grid search optimization consists of evaluating the chosen function $\phi_\lambda(\mathbf{v})$, for a chosen λ, at the $F = 131$ possible frequencies that would separate the two intervals, i.e., a one-dimensional grid search. For $V = 3$ grid search optimization consists of evaluating the function at the $\frac{1}{2}F(F-1) = 8515$ pairs of frequency bins, i.e., a two-dimensional grid search. Grid search optimization for $V > 3$ would also be possible, but turns out to be impracticable due to excessive computational time consumption. Already for the case $V = 3$ optimization by exhaustive grid search consumes several hours of computing time (for the available MATLAB implementation, using a 3 GHz Intel Core Duo CPU with 8 GB RAM).

Instead we have explored alternative procedures for refining the partition of the interval $[f_1 \ f_{V+1}]$ beyond $V = 3$. A natural procedure is given by applying a further grid search optimization to each of the frequency intervals obtained by the first optimization; again each interval may be divided into two subintervals, corresponding to the optimization of one further model parameter (one-dimensional grid search), or into three subintervals, corresponding to the simultaneous optimization of two further model parameters (two-dimensional grid search). Since we hope to identify meaningful frequency intervals, we again choose two-dimensional grid search.

In this paper we report results for the following optimization procedure:

1) two-dimensional grid search optimization of dividing $[f_1 \ f_{V+1}] = [0 \ 500]$ Hz into three intervals, resulting in model parameter vector $\mathbf{v}^{(1)} = \Big(f_2^{(1)}, f_3^{(1)}\Big)$;
2) two-dimensional grid search optimization of dividing each of the intervals $\Big[f_1 \ \ f_2^{(1)}\Big]$, $\Big[f_2^{(1)} \ \ f_3^{(1)}\Big]$ and $\Big[f_3^{(1)} \ f_{V+1}\Big]$ into three subintervals; from the resulting subdivisions, only the subdivision achieving highest increase of $\phi_\lambda(\mathbf{v})$ is kept, while the other two are discarded; the resulting model parameter vector is denoted as $\mathbf{v}^{(2)} = \Big(f_2^{(2)}, f_3^{(2)}, f_4^{(2)}, f_5^{(2)}\Big)$; two of these four parameters are given by $\Big(f_2^{(1)}, f_3^{(1)}\Big)$;
3) each frequency $f_i^{(2)}$, $i = 2, \ldots, 5$, is refined by one-dimensional grid search in the interval $\Big[f_{i-1}^{(2)}, f_{i+1}^{(2)}\Big]$;

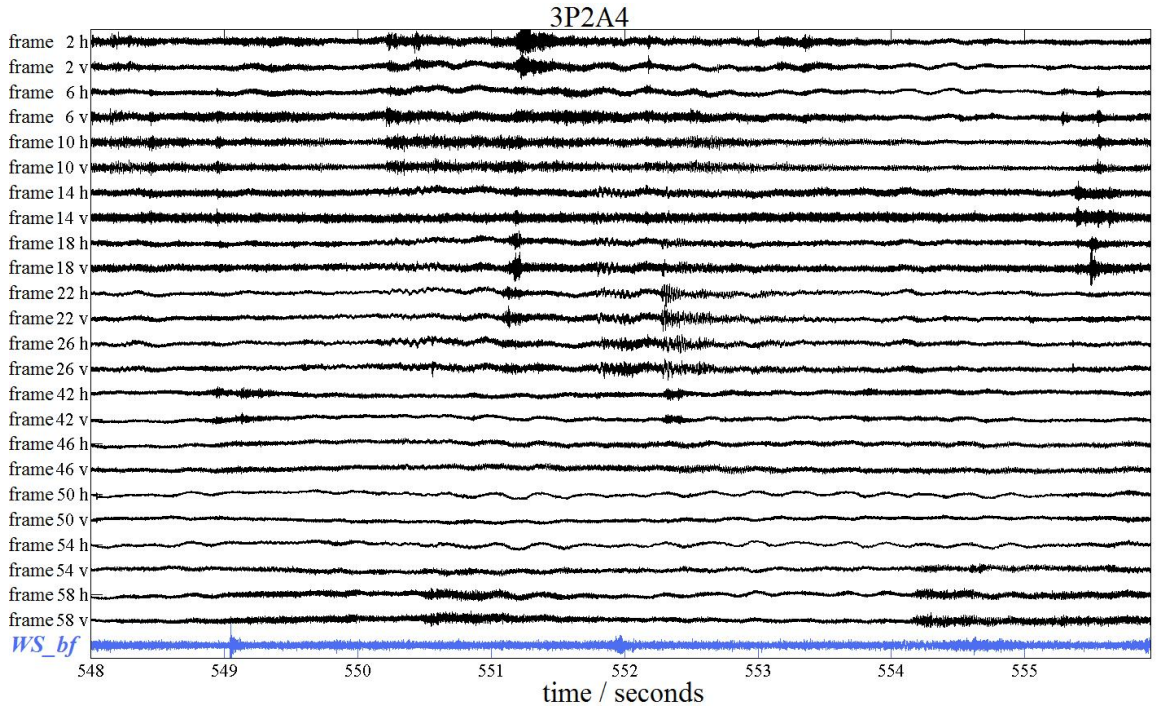

Fig. 6. Data of run "3P2A4" for an interval of 8 s length around the CPA; first 24 time series represent SBS sensors on the hull frames of the ship, while the last time series represents beamformed UWS. Hull frames are labeled by "frame *x*", where *x* is a number, counting from 2 (rear of ship) to 58 (front of ship); the additional letter "h" or "v" refers to horizontal or vertical orientation of the SBS sensors.

4) steps 2. and 3. are iteratively applied three further times to the partition resulting from the previous iteration, resulting in a partition with $V = 11$, represented by model parameter vector $\mathbf{v}^{(5)} = \left(f_2^{(5)}, \ldots, f_{11}^{(5)}\right)$.

The iterative refinement process could be continued beyond $V = 11$, but it would sooner or later lead into overfitting, therefore we decided to stop at an arbitrarily chosen value of $V = 11$. The optimization, as described above, is performed for all values of the regularization parameter λ from the set $\left(2^{-7}, 2^{-6}, \ldots, 2^{7}\right)$.

For the purpose of comparison, we will also show results for equidistant partitions of the interval $[f_1\ f_{V+1}]$, i.e., partitions with parameter vector

$$\mathbf{v}^{(\text{equid.})} = \left(\frac{1}{V} f_{V+1}, \frac{2}{V} f_{V+1}, \ldots, \frac{V-1}{V} f_{V+1}\right)$$

VIII. Results

For each data set ("run") chosen for analysis, and each value of λ, the results of the analysis consist of

- an iteratively refined partition of the interval $[f_1\ f_{V+1}] = [0\ 500]$ Hz into $V = 3, 5, \ldots, 11$ intervals;
- the corresponding values of $\sigma^2_{\text{LS}}(\mathbf{v})$ and $\overline{t^2}_{\text{LS}}(\mathbf{v})$,
- the sets of estimated regression coefficients $\hat{\beta}(c, v)$, of the corresponding estimates of the standard deviations $\hat{\sigma}_\beta(c, v)$ and of the corresponding t-values $t(c, v)$, for each SBS sensor c and each frequency interval v.

We shall visualize the method of analysis, and the typical results, by an example. For this purpose, we choose a run labeled "3P2A4" (see Table 1); the data from a window of 8 s length around the closest point of approach

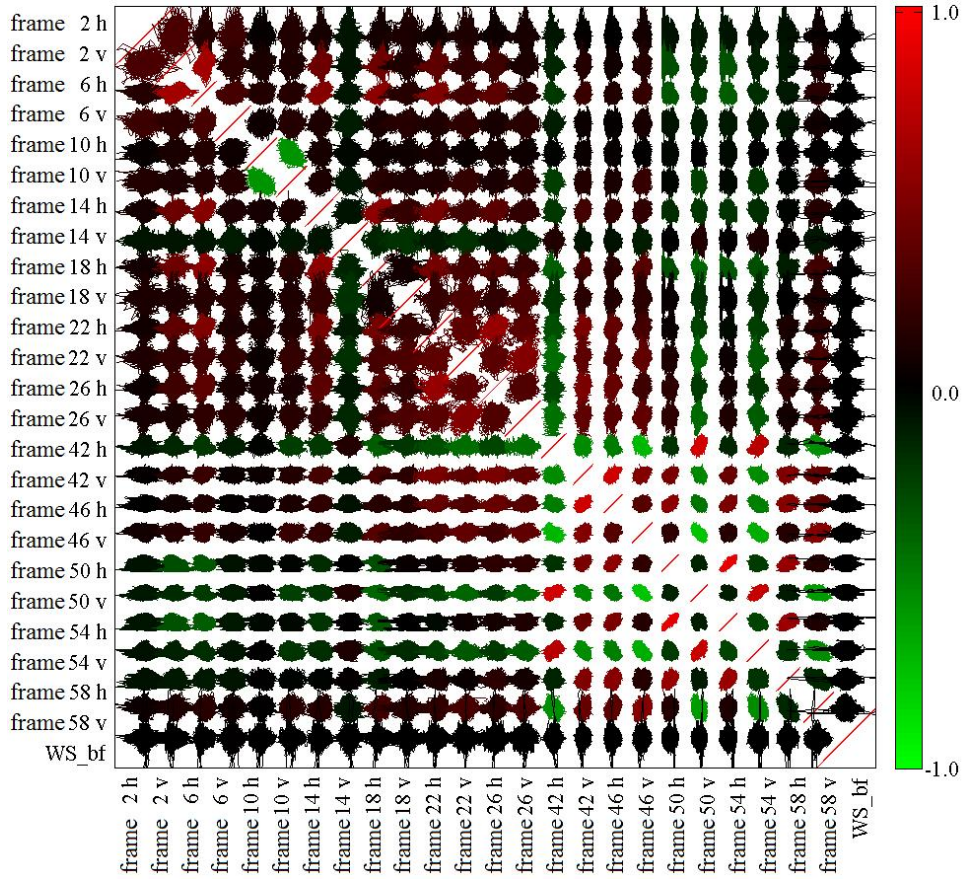

Fig. 7. Perpendicular superpositions of all pairs of data channels for the data displayed in Fig. 6; colors correspond to cross-correlation coefficients (see colorbar at the right).

(CPA) are shown in Fig. 6. The figure shows the SBS data at a set of 24 sensors, and, as the bottommost curve, the beamformed UWS data (labeled "WS_bf"). SBS sensors are ordered from the back of the ship ("frame 2") to the front ("frame 58"); the letters "h" and "v" refer to horizontally and vertically mounted sensors.

Furthermore, in Fig. 7 the perpendicular superpositions of all pairs of data channels are shown (such perpendicular superpositions are sometimes called "scatterplots"). Each pair of channels is color-coded according to the corresponding coefficient of linear cross-correlation. From the figure, it can be seen that there exist only few pairs of channels with strong cross-correlation (except for the positions on the leading diagonal). The largest occuring value of cross-correlation is 0.9054, and the largest occuring value of anti-cross-correlation is -0.7746. In particular, it can be seen that cross-correlations between SBS channels and the beamformed UWS channel are very weak; by systematically changing the steering angle of the beamformer and observing the corresponding changes of the cross-correlations we have ruled out the possibility that these low values of SBS-UWS cross-correlation are an artifact of inappropriate beamforming.

By applying the optimization algorithm, as outlined above, to the given data for regularization parameter values of $\lambda = 2^{-7}, 2^{-6}, \ldots, 2^{7}$, we can compute the L-curve, i.e., the relationship between $\log\big(\overline{t^2}_{\mathrm{LS}}(\mathbf{v})\big)$ and $\log\big(\sigma^2_{\mathrm{LS}}(\mathbf{v})\big)$.

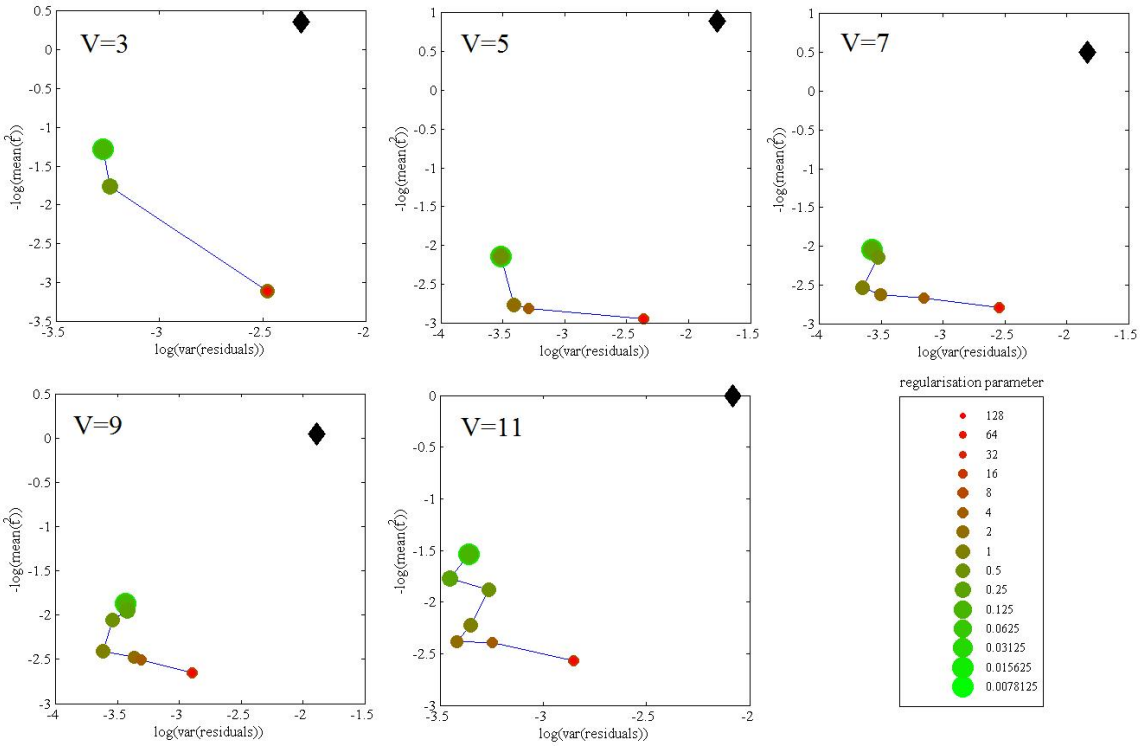

Fig. 8. L-curves for the data displayed in Fig. 6, for $V = 3, 5, \ldots, 11$ intervals; different values of the regularization parameter λ are represented by different size and color of circles (see legend in lower right subfigure); corresponding results for equidistant partitions are represented by black diamonds.

Since usually L-curves refer to quantities which are to be minimized simultaneously, we shall plot the negative of $\log\big(\overline{t^2}_{\mathrm{LS}}(\mathbf{v})\big)$.

The results, for $V = 3, 5, \ldots, 11$ intervals, are shown in Fig. 8, with λ represented by different size and color of circles. The figure also shows the corresponding results for equidistant partitions (black diamonds). In many cases, several values of λ lead to the same partition of the interval, such that the corresponding points in the L-curve coincide; in the figure, such cases can be detected from the different sizes and colors of the circles.

From the figure, it can be seen that the optimized partitions lead to considerably reduced values of $-\log\big(\overline{t^2}_{\mathrm{LS}}(\mathbf{v})\big)$ and $\log\big(\sigma^2_{\mathrm{LS}}(\mathbf{v})\big)$, as compared to the equidistant partitions, i.e., the non-optimized partitions. Furthermore, the curves do indeed have roughly the form of the letter "L". This is a non-trivial result, since conventional regularized regressions do not involve additional numerical optimization steps. Results for the other 4 runs (not shown) are similar, although in a few cases some values of λ behave as "outliers" from the L-curve (usually larger values, $\lambda \geq 32$).

The estimated regression coefficients $\hat{\beta}(c, v)$ and the corresponding estimates of the standard deviations $\hat{\sigma}_\beta(c, v)$ may be visualized as shown in Fig. 9. For this figure we have chosen the example of a partition consisting of $V = 7$ intervals, for a regularization parameter $\lambda = 1$ (roughly corresponding to the value recommended by the L-curve criterion); among the 7 intervals, the regression coefficients for the second interval, corresponding to $[64.8\ 91.6]$ Hz,

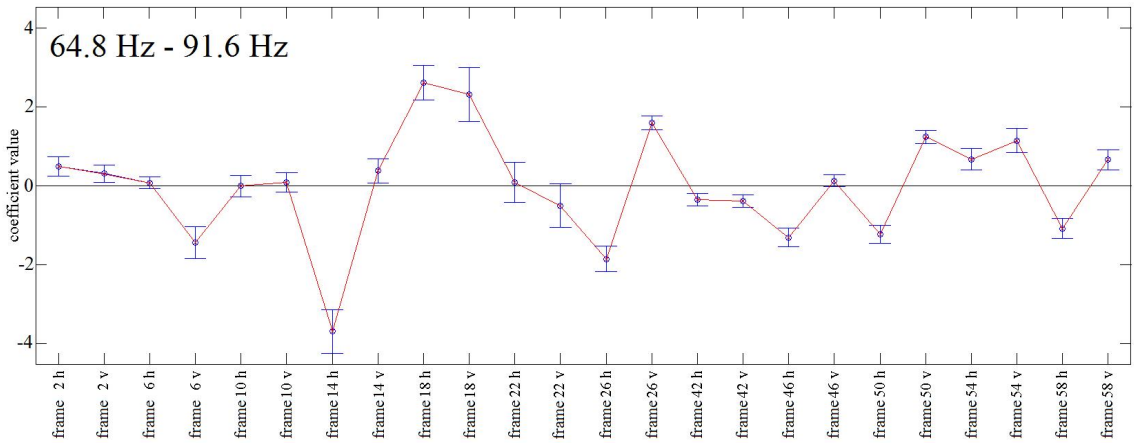

Fig. 9. Estimated regression coefficients $\hat{\beta}(c, v)$ and corresponding 95% confidence intervals (two standard deviations) for the data displayed in Fig. 6, for the second interval, corresponding to $[64.8\ 91.6]$ Hz, of the optimized partition with $V = 7$ and $\lambda = 1$.

are displayed.

From the figure, it can be seen that the regression coefficients scatter within the interval $[-4\ 4]$, with most estimates deviating significantly from zero; t-values are found to be larger than 5 for more than half of regressors. These plots will look different for other intervals; in the present case, this interval was found to achieve highest average significance within the 7 intervals of this partition.

The complete set of estimated regression coefficients $\hat{\beta}(c, v)$ for a given partition may be visualized as shown in Fig. 10. For this figure, the same partition as for Fig. 9 was chosen. The vertical axis of the figure represents the frequency interval $[0\ 500]$ Hz, such that the intervals can be displayed according to their actual size in frequency space; the estimated regression coefficients $\hat{\beta}(c, v)$ are denoted by color coding. As can be seen from the figure, certain combinations of a SBS sensor and a frequency interval stand out by particularly large (absolute) values of $\hat{\beta}(c, v)$. It can also be seen that the optimal partition of the frequency interval $[0\ 500]$ Hz is very different from an equidistant partition, with some very broad, and some very narrow intervals. A similar figure could be created for the t-values; it would show us that the combinations of a SBS sensor and a frequency interval with large (absolute) value of $\hat{\beta}(c, v)$ do not necessarily achieve large t-values.

Furthermore, useful information may be obtained by computing directly the cross-correlations between the regressand and each of the regressors; the corresponding figure is shown as Fig. 11.

The different partitions of the interval $[f_1\ f_{V+1}] = [0\ 500]$ Hz which result from our algorithm, for different choices of λ and V, may be visualized as shown in Fig. 12. In the figure, the frequencies separating the intervals are denoted by triangles. For each value of λ, the first iteration (for $V = 3$) yields a partition defined by the set of 4 frequencies $\left(f_1, f_2^{(1)}, f_3^{(1)}, f_4\right)$, each of which is represented by a triangle. The further iterations for $V = 5, 7, 9, 11$ add further frequencies to this partition, and may also shift some of the frequencies from previous iterations; the corresponding sets of frequencies are displayed to the right of the first set, until the next value of λ is considered.

In Fig. 12, it can be seen that for small values of λ the optimal partitions are essentially identical, until for medium

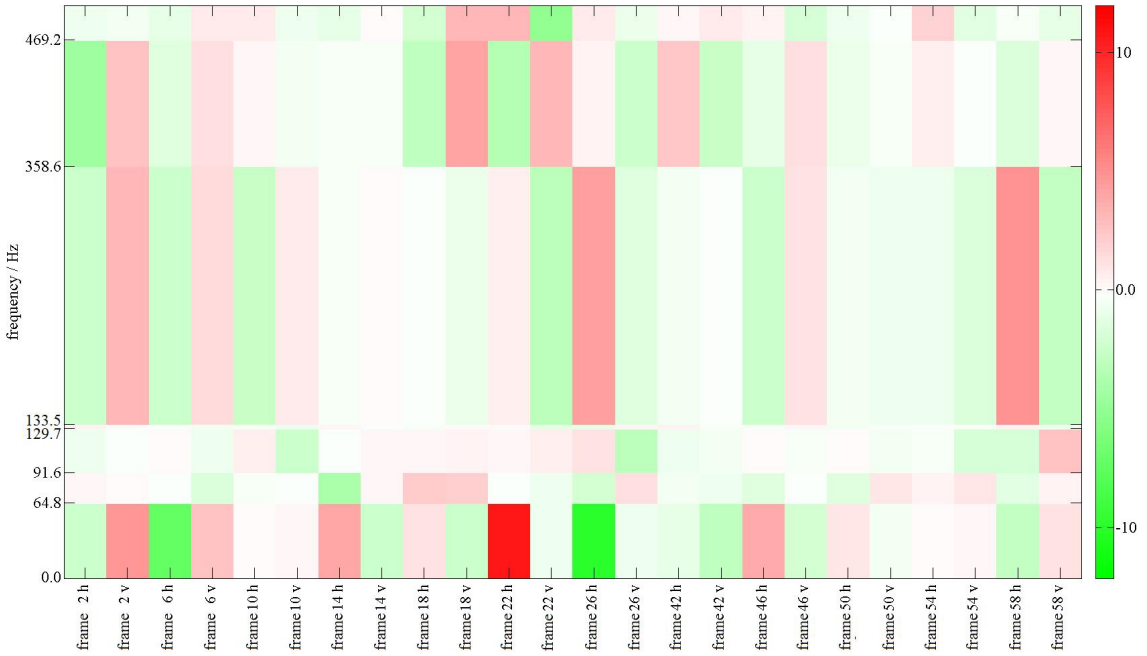

Fig. 10. Estimated regression coefficients $\hat{\beta}(c, v)$ (color-coded, see colorbar at the right) for the data displayed in Fig. 6, for the optimized partition with $V = 7$ and $\lambda = 1$.

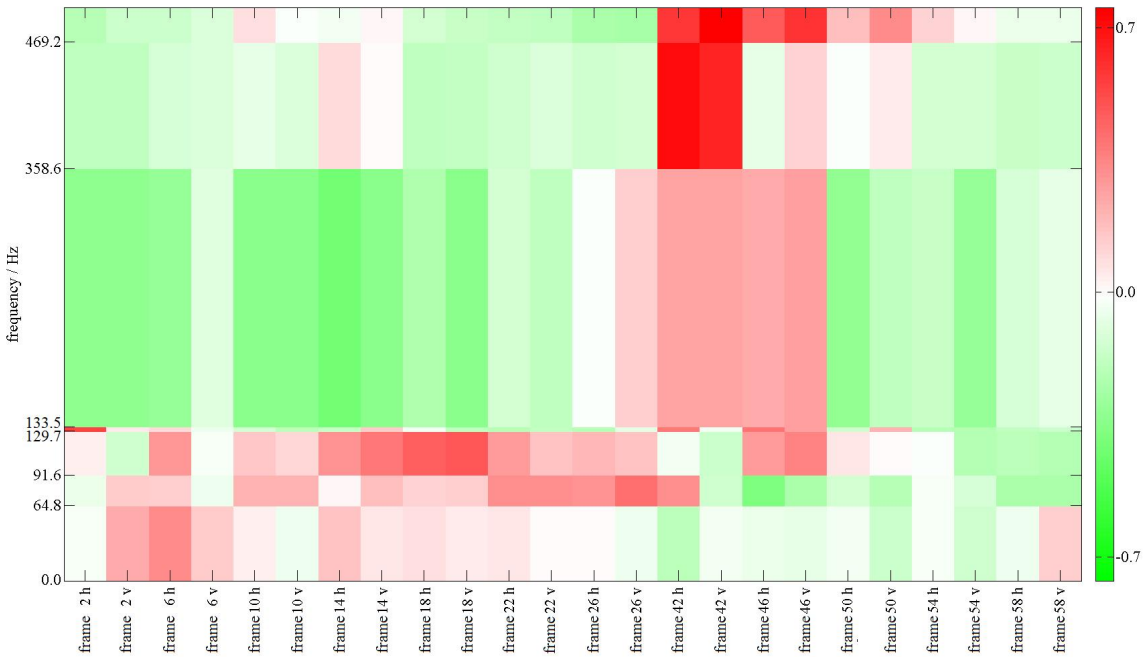

Fig. 11. Cross-correlations (color-coded, see colorbar at the right) for sequences of spectral power based on the data displayed in Fig. 6, for the optimized partition with $V = 7$ and $\lambda = 1$.

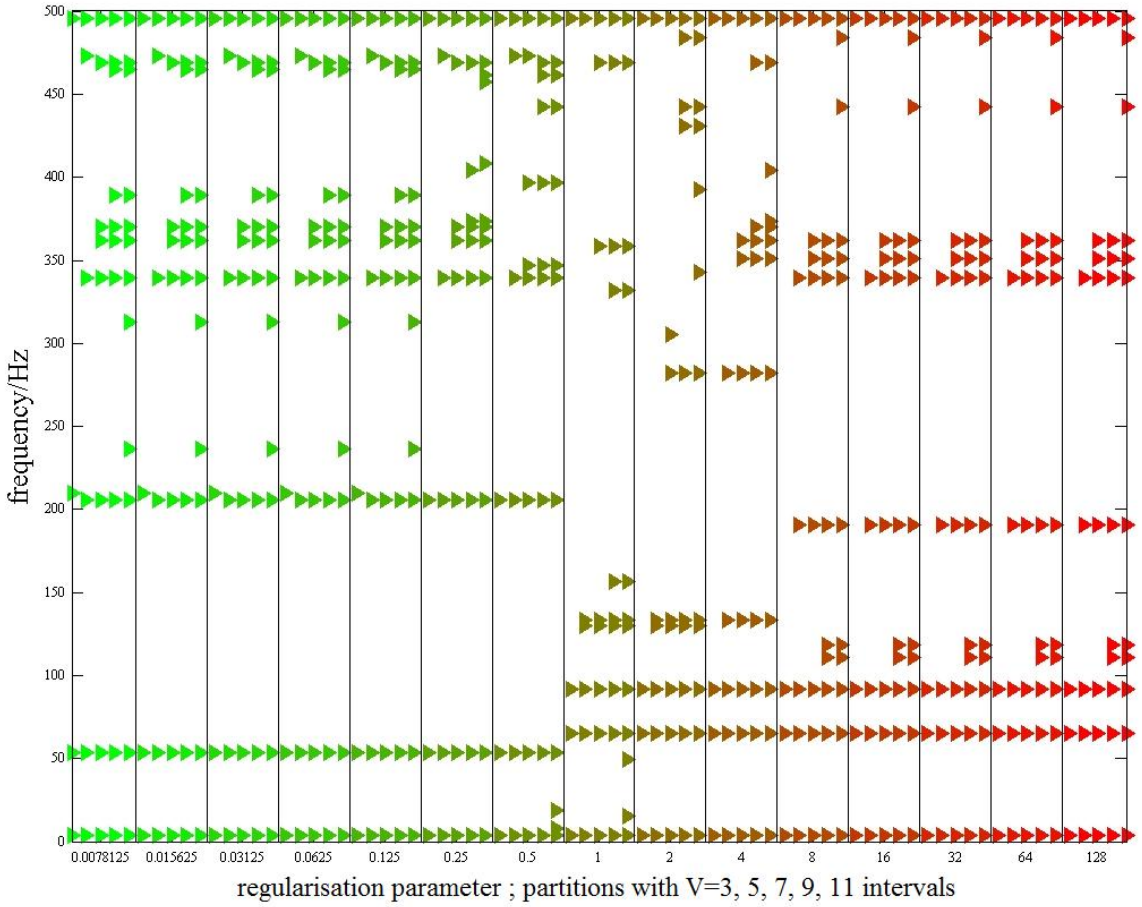

Fig. 12. Optimal partitions of the frequency interval [0 500] Hz for the data displayed in Fig. 6, for regularization parameter values of $\lambda = 2^{-7}, 2^{-6}, \ldots, 2^{7}$ (horizontal axis); for each value of λ partitions with $V = 3, 5, \ldots, 11$ are shown.

values of λ they begin to change considerably; then for large λ again another stable set of optimal partitions results. All optimal partitions have the property in common that they differ markedly from equidistant partitions.

IX. Discussion

We have assumed that much of the power of the recorded UWS time series is caused by the sound generated by the moving ship. However, it would not suffice to study the relationship between SBS and UWS time series by conventional correlation analysis; in fact, such analysis fails to provide meaningful results. As an alternative, one may begin from known oscillations and other technical processes on the ship and aim at detecting the corresponding frequencies in the UWS data. While such approach does have its merits, in this paper we have chosen a fully data-driven approach.

The analysis of the selected runs by the regression-based analysis described above provides a distribution of results that requires further interpretation. While sets of estimated regression coefficients (as displayed in Fig. 10) refer to the corresponding sets of given regressors, cross-correlations (as displayed in Fig. 11) refer to individual pairs of a regressand and a regressor, therefore they provide an alternative view on the coupling between SBS and

UWS. For this reason, the figures of both sets of measures may differ considerably for the same run. Nevertheless, the regression step itself remains necessary, in order to optimise the frequency partitions.

Fig. 13 shows the cross-correlations between regressand and regressors for run 3P2A4 for optimized partitions with $V = 11$ and different values of λ, namely small values of λ (which all lead to the same partition), $\lambda = 1$ (the value recommended by the L-curve), and large λ (again leading to the same partition). The figure also shows the cross-correlations for the case of an equidistant partition (bottom right subfigure). As can be seen in this figure, for this run the existence of a group of strong positive cross-correlations at some forward SBS sensors and frequencies larger than 350 Hz represents a very persistent feature that can even be found in the equidistant partition. This persistency of main features is also found for other runs; the same is also found for the regression coefficients.

The different partitions shown in Fig. 13 may either be compared by the statistical criterion of Equation (7), in combination with the L-curve approach, or by visual evaluation. From the statistical criterion it is clear that the data-adaptive optimized partition with $n = 1$ (top right subfigure) represents the best choice; it can be seen from the positions of the black diamonds in Fig. 8 that the equidistant partition is inferior for all V and n. By visual evaluation it can be seen that for the equidistant partition the pattern of correlated (red) and anti-correlated (green) fields appears less ordered than for the data-adaptive optimized partitions. Since such ordering will not occur by chance, we believe that data-adaptive optimized partitions allow a better representation of the available information than equidistant partitions.

When two runs which were recorded under the presence of very similar physical conditions, are compared, similar results are obtained; as examples we show in Fig. 14 the pairs (3P6B1, 3P6B3) and (3P3B3, 3P3B5) measured at a speed of 8 knots and 15 knots, respectively. Both pairs have pronounced positive cross-correlations steering on the rear part of the ship. The agreement of the results within a pair of runs measured at the same speed is found to be better at moderate speeds where internal SBS sources play a more important role [1]. At large speed external sources, such as flow noise [18], become more relevant. Those contributions may not have been captured comprehensively by the SBS sensors, since they originate from outside of the ship's hull.

While pure power spectra are fairly well reproducible for different runs with similar state of the ship, here we find that for this analysis of the coupling between SBS and UWS results are less well reproducible. This finding can be interpreted partly as a consequence of analyzing a more complicated phenomenon, i.e., the correlations between two different sets of recordings, which may be more susceptible to changes of ambient conditions. For the first pair (3P6B1, 3P6B3) the state of the ship was not exactly the same (see difference of rotation rate, as given in Table 1), so a certain amount of differences can be expected. For the second pair (3P3B3, 3P3B5) the state of the ship was nominally the same. However, it has to be emphasized that for experiments at sea it is impossible to reproduce ambient conditions exactly: wind and weather conditions are always changing gradually; between both runs, a time of approximately 30 minutes had passed. Also other parameters, such as the distance between ship and array, and the exact course of the ship cannot be reproduced precisely. The situation is intrisically different from a well controlled experiment within a lab. Therefore, when employing a highly sensitive method of analysis, it is unavoidable that results differ to a certain extent even for pairs of runs with (nominally) identical state of the ship.

On the other hand, when comparing the cross-correlation results between the pairs (3P6B1, 3P6B3) and (3P3B3,

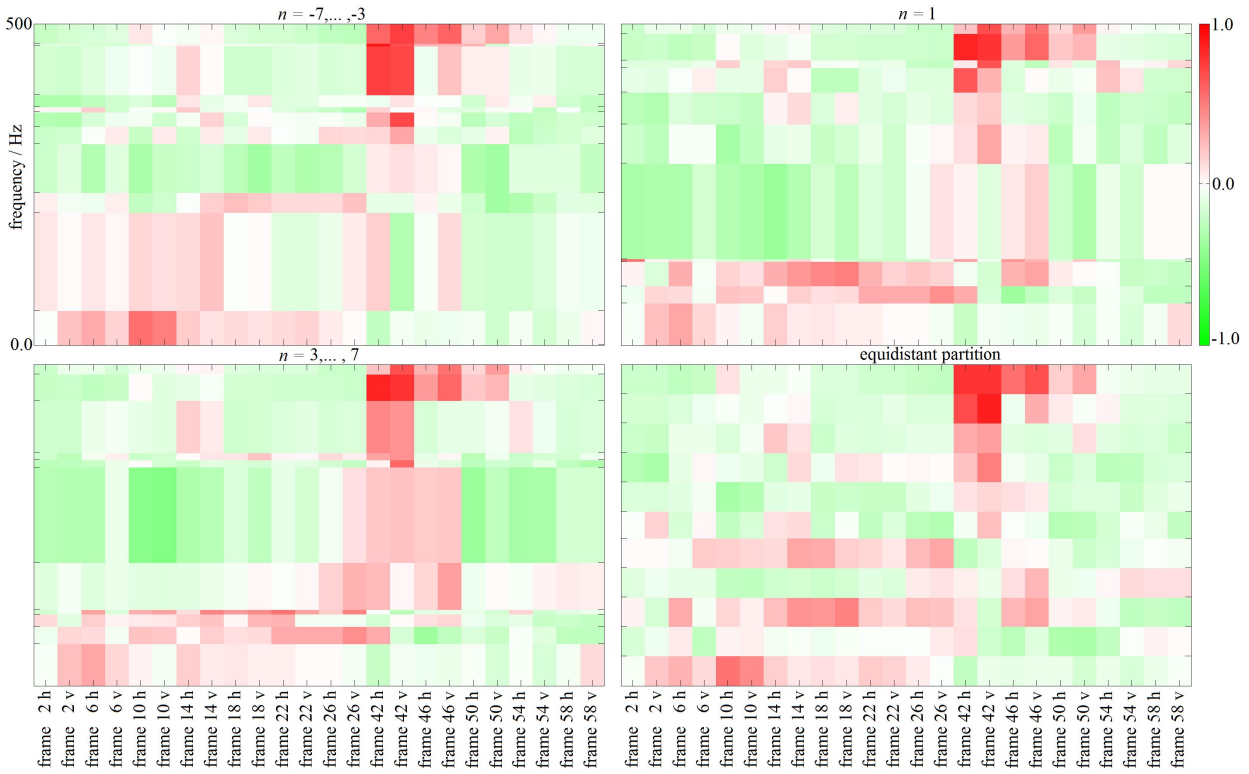

Fig. 13. Cross-correlations (color-coded, see colorbar at the right) for sequences of spectral power for the data displayed in Fig. 6, for optimized partitions with $V = 11$ and $\lambda = 2^n$, where n is given above each subfigure. The subfigure in the bottom right position represents the equidistant partition for $V = 11$.

3P3B5), we notice significant differences. These differences obviously reflect the differences of the physical conditions present during these runs, with respect to speed and internal state of the ship. This can be seen clearly for the cross-correlations above 300 Hz in the rear part of the ship for higher speed. However, relatively little difference can be seen in the bow part of the ship; we believe that the reason is given by the fact that a SWATH ship creates only minor bow wave effects, therefore at higher speed there is only little increase of flow noise in the bow part.

X. Conclusion

Ships behave as complex sound sources, generating acoustic emissions composed of a variety of different contributions. From the viewpoint of naval applications, the ability to predict the (instantaneous) underwater signature in the far-field from information available on-board would be desirable. This information is, of course, only a proxy and the coupling to the emitted underwater sound needs to be determined. We have presented results on investigating the coupling of SBS and UWS time series, based on the analysis of data sets gained from an open-sea experiment with RV PLANET and a freely drifting vertical array buoy. The SBS data were measured on the submerged part of the ship's hull, since the vibration behavior of the hull determines, in principle, the sound radiated into the surrounding water. For this purpose we have introduced an approach to determining optimal partitions of the

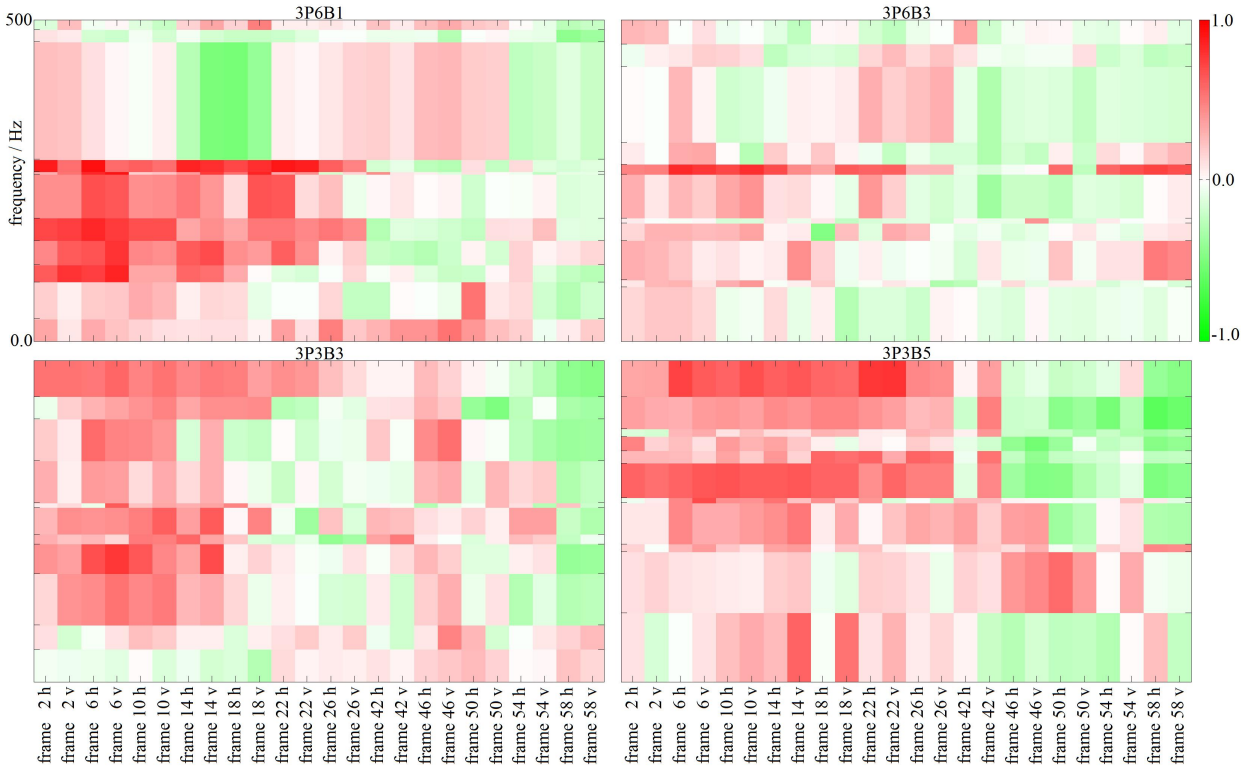

Fig. 14. Cross-correlations (color-coded, see colorbar at the right) for sequences of spectral power based on the data from 4 selected runs, for the optimized partition with $V = 7$ and $\lambda = 2^{-7}$. All vertical axes range from 0 Hz to 500 Hz.

relevant frequency range $[0\ 500]$ Hz into intervals, such that sequences of spectral power can be generated for each frequency interval and each SBS sensor, as well as for the beamformed UWS time series.

The main contribution of this paper is a practicable algorithm for determining optimal partitions in frequency space; for the experimental data analyzed in this paper, we have found that, from a statistical point of view, equipartition is not optimal, while non-equidistant data-adaptive frequency bands provide a better representation of the available information. Furthermore, we have observed that for pairs of runs with similar physical state of the ship the resulting maps of cross-correlation are not well reproducible, although some similarities can be seen. However, this is only a preliminary result, based on the analysis of a limited amount of data (two times two similar runs); more data needs to be recorded and analyzed.

We hope that the optimization approach introduced in this paper will contribute to obtaining better characterisations of the acoustic state of ships and, moreover, be useful as a preprocessing step for a prediction method of the underwater signature from structure-borne sound measurements. This issue will be addressed in future work.

REFERENCES

[1] D. Ross. *Mechanics of underwater noise*. Pergamon Press, New York, 1972.

[2] R.J. Urick. *Principles of underwater sound*. Peninsula Publishing, Los Altos (CA), 1983.

[3] M.C. Junger and D. Feit. *Sound, structure, and its interaction*. MIT Press, Cambridge (MA), 2.ed., 1986.

[4] P.H. Dahl, J.H. Miller, D.H. Cato, and R.K. Andrew. *Underwater ambient noise*. Acoustics Today, 2, 23-33, 2007.

[5] W.M. Carey and R.B. Evans. *Ocean ambient noise: Measurement and theory*. Springer, New York, 2011.

[6] P.T. Arveson and D.J. Vendittis. *Radiated noise characteristics of a modern cargo ship*. J. Acoust. Soc. Am., 107, 118-129, 2000.

[7] Ch. Erbe, A. MacGillivray, and R. Williams. *Mapping cumulative noise from shipping to inform marine spatial planning*. J. Acoust. Soc. Am., 132, EL423-EL428, 2012.

[8] M.F. MacKenna, D. Ross, S.M. Wiggins, and J.A. Hildebrand. *Underwater radiated noise from modern commercial ships*. J. Acoust. Soc. Am., 131, 92-103, 2012.

[9] P. Scrimger and R.M. Heitmeyer. *Acoustic source-level measurements for a variety of merchant ships*. J. Acoust. Soc. Am., 89, 691-699, 1991.

[10] S. Wales and R. Heitmeyer. *An ensemble source spectra merchant ship radiated noise*. J. Acoust. Soc. Am., 111, 1211-1231, 2002.

[11] D.K. Wittekind. *A simple model for the underwater noise source level of ships*. J. Ship Prod. Des., 30, 1-8, 2014.

[12] M. Zampolli, A. Tesei, G. Canepa, and O.A. Godin. *Computing the far field scattered or radiated by objects inside layered fluid media using approximate Green's functions*. J. Acoust. Soc. Am., 78, 4051-4058, 2008.

[13] J.D. Maynard, E.G. Williams, and Y. Lee. *Near-field acoustic holography: I. Theory of generalized holography and the development of NAH*. J. Acoust. Soc. Am., 78, 1395-1413, 1985.

[14] V. Nejedl, A. Stoltenberg, and J. Schulz. *Free-field measurements of the radiated and structure-borne sound of RV "PLANET"*. Proc. 11th Europ. Conf. Underwater Acoustics, 2-6.7.2012, Edinburgh, 814-821, 2012.

[15] B.R. Hendriks, Z.A. Daya, L. Kätow, D. Fraedrich, F.M. Talbot, C.A.F. de Jong, T.C. Richards, A. Constable, L. Gilroy, M. Nakjem, S. Schäl, T. Krämer, B. Rasch, J.-M. Chapelier, J.B. Nelson, D. Rog, J.C.J.G. Withagen. *Q340 Cruise Plan / RIMPASSE 2011 Trial Plan, (Radar Infra-red Electro-Magnetic Pressure Acoustic Ship Signature Experiments)*. Technical Note, DRDC Atlantic TN 2011-151, June 2011.

[16] P.J. Huber. *Robust statistics*. Wiley, New York, 1981.

[17] Z.B. Zabinsky. *Stochastic adaptive search for global optimization*. Springer Science & Business Media, 2003.

[18] C. de Jong, J. Bosschers, H. Hasenpflug, and T. Farabee. *Surface ship underwater radiated flow noise*. Proceedings of UDT Europe, Amsterdam, 21-23.6.2005.